AIAA AVIATION Forum
June 25-29, 2018, Atlanta, Georgia
2018 AIAA/CEAS Aeroacoustics Conference

10.2514/6.2018-3123

Acoustic Localization of Gunshots in the Presence of Obstacles

Aniruddha Sinha* and Tushar Singh†
Dept. of Aerospace Engineering, Indian Institute of Technology Bombay, Mumbai 400076, INDIA

Acoustic localization of gunshots is of interest for protecting security camps in contested forests, increasing soldiers' situation awareness in ambushes, as well as in guarding cities. All these scenarios are also fraught with obstacles coming in the path of acoustic waves. We present a computational study of the effect of obstacles on the accuracy of localization of point sound sources like gunshots. The two-dimensional linearized Euler equations are solved with the dispersion relation preserving scheme. The localization is performed using the wavefront curvature method based on pressure signatures recorded at three virtual microphones. We report at most 8° of error in the estimated bearing angle of the source across a range of practical values of five parameters – viz. the location and size of the obstacle, and the size, orientation and location of the sensor array relative to the source. This level of error may be quite acceptable in the scenarios considered. On the other hand, the range error is much more severe, exceeding 100% of the true range in a few cases. In the scenarios considered, the bearing angle estimate is much more critical than the range estimate. Overall, we conclude that acoustic localization approaches are quite robust in the presence of obstacles.

I. Introduction

Modern gun-battles are rarely waged on open ground where enemies face each other, and the origin of unfriendly and friendly fire is easy to locate. Instead, most gunfires are encountered in obstacle-dense situations like cities, forests and mountain valleys, where the location of a shooter may be difficult to pinpoint aurally. Moreover, security forces may not even be present within audible range of all gunshots at all times, due to the highly mobile nature of modern combat. However, in these situations, it would still be desirable to have real-time knowledge of the origin of unfriendly fire so as to prepare prompt and effective counter-measures.

Gunshots have two unique acoustic features that are used to localize their origin – these are the muzzle blast and the shock wave trailing the bullet if it is travelling supersonically. In this work we focus on the former signature only. A conventional firearm uses an explosive propellant in its muzzle to discharge the bullet. The sound from this explosion travels in all directions at sonic speed, but is loudest in the direction of firing. Also, the typical acoustic signature varies across observer locations [1]. The microphone signal recorded in the front sector of the gun displays a sharp rise (within 50 to 200 μsec) followed by a relatively slower decay. The signature recorded in the rear sector shows several oscillations that are much less distinctive. The blast wave suffers attenuation and broadening due to atmospheric absorption, wind, ground effects, and hindrance from solid obstacles – this renders them less useful for sensors at large distances from the shooter. As a practical matter, the bearing angle of the gunfire source is more relevant than its range.

The literature reports several algorithms for the problem of locating the shooter using the muzzle blast alone; the choice is usually dictated by the particular use-case scenario and the sophistication of the hardware implementation. The basic input to all the algorithms is the set of differential times-of-arrival (DTOAs) of the acoustic event wavefront for various pairs of sensors. Some of the available algorithms are the classical least-squares method with a regularization term [2], Bancroft's method [3], wavefront curvature method [4,5], and unit sighting vector method [6]. The last three methods yield a closed-form solution, whereas the first one is

*Assistant Professor; AIAA Member; Corresponding author: as@aero.iitb.ac.in
†Research Assistant

iterative. The first three methods assume that the acoustic wavefront is spherical, and they yield the bearing angle and range of the acoustic source. The last algorithm assumes that the source is so far away from the sensors that the wavefront is plane, thereby yielding the bearing angle only; however, the range may be estimated if more than one cluster of sensors are deployed far enough apart. In two-dimensional problems where the source may be assumed to be coplanar with the sensors, at least three sensors are needed for all the algorithms; the first two algorithms can readily utilize data from more sensors to improve the accuracy. In three-dimensional problems, at least one more sensor is needed.

All the available algorithms have been developed for acoustic environments that are free from obstacles. In other words, each sensor is assumed to have a line-of-sight to the source. In this work, we intend to understand the effect of obstacles on localization of acoustic events. For this, we use an in-house code to solve the linearized Euler equations on a uniform Cartesian grid using the dispersion-relation-preserving (DRP) scheme[7]. Given the limitations of the code, only rectangular obstacles can be simulated. The wavefront curvature method is used for localization of the simulated acoustic event.

II. Computation of two-dimensional acoustics in the presence of obstacles

Linear acoustics are a solution of the linearized Euler equations (LEE). An in-house LEE code was developed following Ref. 8. The salient features of this code are listed below; further details of the implementation may be found in the reference.

- The two-dimensional equations are solved.
- The grid is Cartesian, and is uniform in both x and y directions.
- The 7-point (fourth-order accurate) optimized finite difference scheme is used for spatial discretization.
- The four-level optimized time-marching scheme is used.
- There is provision for imposing a uniform base flow in the domain. However, in the presence of obstacles, the base flow is turned off since its uniformity is unphysical.
- The far field can have radiation or inflow boundary conditions; the latter only applies in case of a non-zero base flow.
- The presence of one or more obstacles may be simulated, as long as their edges coincide with the uniform background grid. Thus, only rectangular obstacles can be considered. The walls of the obstacle have perfectly reflecting boundary conditions.
- Spurious short waves that contaminate the solution are especially problematic near the corners of obstacles; artificial selective damping with mesh Reynolds number of 20 is applied to address this.

LEE supports vorticity and entropy modes along with acoustic modes. The latter can be selectively triggered by specifying only the pressure initial condition while the remaining variables (x and y components of velocity, and density) are set to zero[8]. In the code, all length dimensions are normalized by the x-grid spacing Δx; the y-grid also has the same spacing. All velocities are normalized by the speed of sound c, and density is normalized by ambient density ρ_0. Pressure is normalized by $\rho_0 c^2$.

The acoustic solution was validated against the ones reported in the textbook for the case of free space propagation and the case of an infinite wall on one side, both with an imposed base flow.

III. Wavefront curvature method

The wavefront curvature method[4,5] is a passive ranging method used to localize acoustic sources assuming perfectly spherical spreading of the acoustic wave. The idea is to find the curvature of the wavefront generated by the acoustic event of interest that passes over a set of three acoustic sensors in a planar problem (see the schematic in fig. 1). The acoustic wave radiated by the source will be received at the different sensors at slightly different times. The differential time-of-arrival (DTOA) for two pairs of sensors ($S_0 - S_1$ and $S_0 - S_2$ in the schematic) are determined from the recorded sound signals, and the range and bearing of the acoustic source is recovered from them.

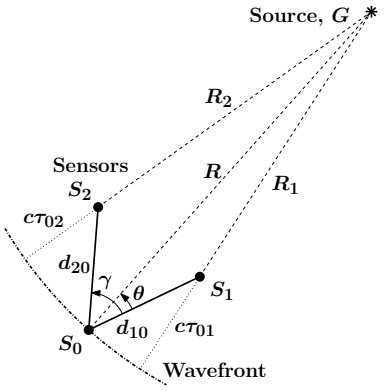

Figure 1: Schematic for application of wavefront curvature method to a non-linear array

In the schematic of fig. 1, the origin of the sensor triplet is S_0, and its axis is $S_0 - S_1$. With respect to this, the range is R and the bearing angle is θ. To calculate these two quantities, we first define the DTOA between a pair of sensors with indices i and j as $\tau_{ij} := t_i - t_j$, where t_i is the time-of-arrival of the wavefront at sensor i. We also define the normalized DTOA between the sensor pair $i - j$ as $\eta_{ij} := c\tau_{ij}/d_{ij}$, where c is the speed of sound in the ambient and d_{ij} is the separation between the sensor pair $i - j$. Note that η_{ij} takes values between -1 and $+1$. In particular, $\eta_{ij} = +1$ indicates that the source, sensor j and sensor i is an ordered collinear triplet. Similarly, $\eta_{ij} = -1$ indicates that the source, sensor i and sensor j is an ordered collinear triplet. Finally, $\eta_{ij} = 0$ indicates that the source is on the perpendicular bisector of the line joining sensors i and j.

From the assumption that the wavefront is spreading spherically at the uniform speed of sound, and from the geometry of fig. 1, we have

$$R_1 = R - c\tau_{01} = R + c\tau_{10}. \tag{1}$$

An alternate expression for R_1 is obtained from the cosine law for the triangle GS_0S_1, viz.

$$R_1 = \sqrt{R^2 + d_{10}^2 - 2Rd_{10}\cos\theta}. \tag{2}$$

Eliminating R_1 from the above two equations along with the use of the definition of η_{ij} yields

$$R = d_{10}\frac{1 - \eta_{10}^2}{2(\eta_{10} + \cos\theta)}. \tag{3}$$

With reference to fig. 1, a similar analysis of the sensor pair $S_0 - S_2$ yields

$$R = d_{20}\frac{1 - \eta_{20}^2}{2(\eta_{20} + \cos(\gamma - \theta))}, \tag{4}$$

where γ is the included angle in the array (positive if the arm $S_0 - S_1$ has to be rotated counter-clockwise to encounter the arm $S_0 - S_2$, as in fig. 1).

To solve for the bearing angle, one can eliminate the range R from eqns. (3) and (4). Use of trigonometric identities then yields the solution for the bearing angle as

$$\theta = \tan^{-1}\left(\frac{\sin\gamma}{\cos\gamma - \mathscr{A}}\right) \pm \cos^{-1}\left(\frac{\mathscr{A}\eta_{10} - \eta_{20}}{\sqrt{1 + \mathscr{A}^2 - 2\mathscr{A}\cos\gamma}}\right), \qquad \mathscr{A} := \frac{d_{20}(1 - \eta_{20}^2)}{d_{10}(1 - \eta_{10}^2)}. \tag{5}$$

This expression is evidently invalid if $\eta_{10} = +1$ or -1, but in the respective cases the bearing angle θ is π and 0, as discussed earlier. Similarly, if $\eta_{20} = +1$ or -1, θ is easily seen to be $\gamma + \pi$ and γ respectively.

Substitution of the two solutions for the bearing angle in eqn. (3) (or eqn. (4)) yields two corresponding solutions for the range R. In most cases, substitution of these two (θ, R) solution sets in the original equations will reveal only one of them to be valid. However, under degenerate circumstances, the wavefront curvature method (and in fact any algorithm) with a sensor triplet yields two solutions, and more sensors are required to resolve the ambiguity.

For the consistency of subsequent reporting, the reference point in the sensor array is taken to be its centroid instead of the 0th sensor.

IV. Results

We first demonstrate the effect of obstacles on the acoustic field of a point source; subsequently we present the result of a parametric study on the localization accuracy in the presence of an obstacle.

It will be shown below that acoustic waves resembling typical muzzle blasts are obtained in the far field by choosing a Gaussian pulse as the initial condition for pressure (as in Ref. 8)

$$p(x, y, t = 0) = \varepsilon \exp\left[-\ln 2 \left\{(x - x_0)^2 + (y - y_0)^2\right\} / \sigma^2\right]. \tag{6}$$

Here, σ determines the spatial width of the pulse and is set to 3 units following Tam [8]; the implications of this choice will be discussed subsequently. For the amplitude ε, a normalized value of 0.01 was used; note that this must be small compared to unity for linearity to hold. The origin of the pulse (x_0, y_0) is set to the origin of the coordinate system. The time step is chosen as $0.1\Delta x/c$; Tam [8] recommends an upper bound of $0.19\Delta x/c$ for stability.

A. The nature of acoustic distortion caused by obstacles

Figure 2a shows the contours of pressure fluctuations in the domain at several time instants in the absence of any obstacle. The smooth behaviour of the expanding pressure pulse near the boundaries ($130\Delta x$ from the source in all directions) attest to the correct implementation of the radiating boundary condition. Figure 2b presents the corresponding results when a small square obstacle of size $20\Delta x$ on a side is centred at $(20\Delta x, 0)$. Figure 2c shows the pressure contours when the obstacle is doubled in size and is centred at $(30\Delta x, 0)$. The increasing distortion of the wavefront is apparent in these figures, along with the reflected and diffracted waves. Evidently, the distortion is pronounced directly across from the obstacle, on the other side from the source. However, the distortion diminishes with distance from the obstacle.

Figure 3a displays the pressure signatures recorded on three virtual microphones in the case of propagation in free space. The signals exhibit a single sharp positive excursion followed by a single negative excursion that is more gradual, similar to typical muzzle blast signatures [9]. This justifies the use of the Gaussian pulse as the initial condition. The distortion and attenuation of the acoustic wave in the presence of the obstacle is clearly demonstrated in fig. 3. The reflected wave is evident in the case of the small obstacle; it has superposed with the primary wave and obliterated the negative peak in the case of the large obstacle.

The localization approach requires the differential time-of-arrival (DTOA) for all sensor pairs, which is identified as the time delay corresponding to the peak of the cross-correlation of the corresponding signal pair. Quadratic interpolation is used to refine the estimate of the peak time delay from cross-correlation.

We estimate the time period of the pulse to be about $12\Delta x/c$ (the time from the positive peak to the negative peak is half of this), so that its wavelength is $\lambda = 12\Delta x$. For reference, the time period of muzzle blasts reported in the literature (e.g. Ref. 1,9) is approximately 3 msec; this corresponds to a wavelength of about 1 m. In the rest of the paper, the above wavelength will be used to non-dimensionalize all linear dimensions, e.g., obstacle size, sensor array size, array-to-source distance, and obstacle-to-source distance.

B. Parametric study of localization error due to obstacles

Sensor-to-source distance: If the source is very close to the sensor array, then the algorithmic localization is redundant – aural and visual discrimination is sufficient in this context. On the other hand, as we have alluded to in the context of fig. 2 and will quantify subsequently, the deleterious effect of an obstacle on localization accuracy diminishes with distance of sensors from the source. Keeping in mind the computational cost, we initially study the case where the sensors are about 48λ from the source. Per the preceding discussion, this corresponds to a physical distance of about 48 m. Subsequently, we also report on simulation results using an array placed 30λ from the source.

Sensor array size: Table 1 gives the configuration of four sensor triplets that we consider. The arrays are all isosceles triangles; equilateral triangles were aimed for, but could not be achieved exactly given the limitations of the square structured grid of the simulation. The triplets are arrayed either symmetrically or asymmetrically about the $x-$axis – the arrays are named accordingly. Two array sizes – $\lambda/2$ and λ – are evaluated, these being the measure of the base of the isosceles triangle. These correspond to ~ 0.5 m and ~ 1 m physical arrays.

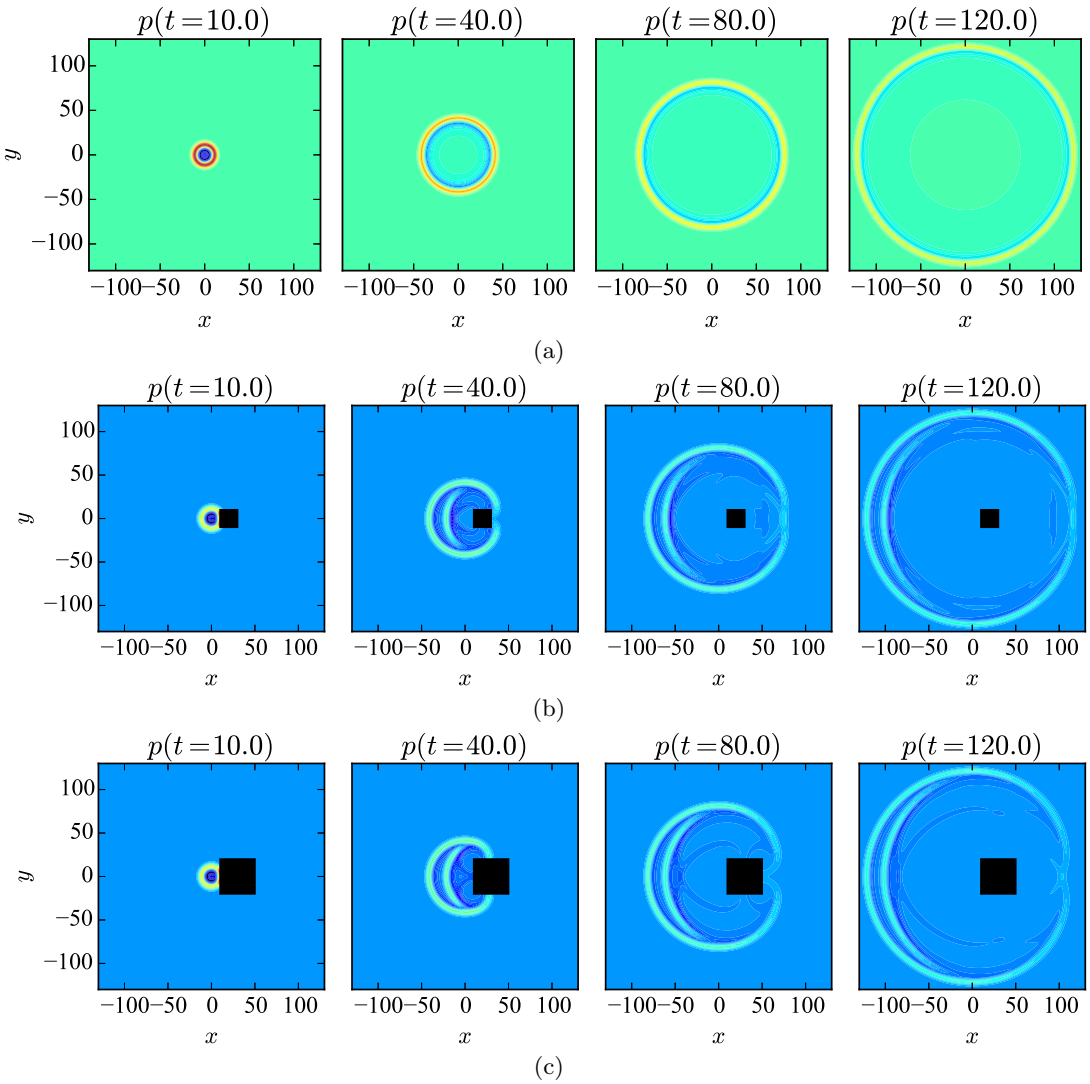

Figure 2: Contours of pressure at various time instants (a) in free space, and in domains with (b) a small obstacle and (c) a large obstacle. Sub-plots in each row have a common colour scale; coordinates x and y are normalized by the grid spacing Δx; time t is normalized by $\Delta x/c$.

Obstacle size: Square obstacles of four different sizes – $\lambda/2$, λ, 2λ, 3λ – are assessed. These correspond to a range of ~ 0.5 m to ~ 3 m. As expected, and demonstrated below, the localization accuracy degrades with the obstacle size. Obstacles of even larger size are not of practical interest in the context of a forest environment, say. In a city setting, the problem is highly three-dimensional, and thus the present exercise is insufficient anyway.

Obstacle location: The discussion Section A has indicated that the distortion of acoustic waves due to an obstacle is primarily confined to the zone directly behind the obstacle. Thus, in the parametric study that follows, we place obstacles on or near the line joining the source to the sensors. As a practical matter, one will not situate a sensor array close to an immovable obstacle. Thus, the minimum range of along-the-line distances between the obstacle and sensor array is limited to 15λ. Four different along-the-line ($x-$coordinate) obstacle positions are evaluated – viz. 3λ, 7λ, 11λ, and 15λ from the source. Also, four different normal-to-the-line ($y-$coordinate) positions are evaluated – viz. 0λ (on the line), λ, 2λ and 3λ.

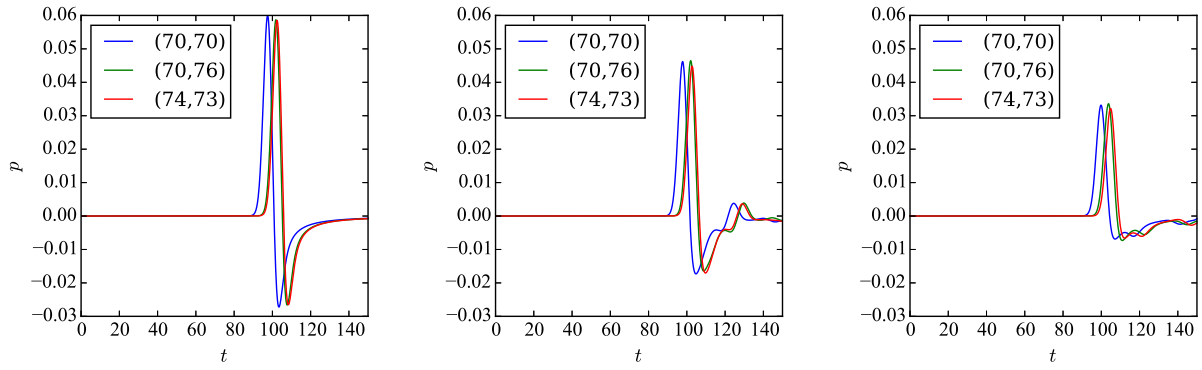

(a) (b) (c)

Figure 3: Timeseries of pressure (normalized by the ambient pressure) recorded at three virtual probes with coordinates (in units of Δx) as noted in the legends; time t is normalized by $\Delta x/c$. Displayed are the cases of (a) free space, (b) small obstacle, and (c) large obstacle, as presented in fig. 2.

Array	**Symmetric, size $\lambda/2$**			**Symmetric, size λ**			**Asymmetric, size $\lambda/2$**			**Asymmetric, size λ**		
Probe	0	1	2	0	1	2	0	1	2	0	1	2
$\boldsymbol{x}$	48	48	48⅓	48	48	48⅔	47¼	48¼	48	47½	48½	48
$\boldsymbol{y}$	$-1/4$	¼	0	$-1/2$	½	0	$-1/6$	$-1/6$	1/6	$-1/3$	$-1/3$	⅓

Table 1: Virtual probes' x and y coordinates in units of pulse wavelength λ for four arrays considered – two arrays that are symmetric about the $x-$axis, and two that are not. All arrays are $\sim 48\lambda$ from the source, and centered on the $x-$axis.

1. *Bearing angle estimation error*

Figure 4 presents the bearing angle estimation errors corresponding to the ($4^4 =$) 256 parameter combinations described above. The maximum error is limited to only 3° over all the cases analyzed. None of the trends discernible in the results are absolute, attesting to the complicated nonlinearity of the localization problem.

No error is incurred in the case of a sensor array situated symmetrically about the line joining the source to the array centroid, with the obstacle positioned symmetrically on the line ($y = 0$). This is to be expected, since the array encounters a symmetrically distorted acoustic field. Such is not the case when the sensors are arrayed asymmetrically about the line from the source.

In the case of the symmetric array, the errors are quite similar for the two array sizes studied. On the other hand, for the asymmetric array case, the error increases with decreasing array size, which is the expected trend. As anticipated from fig. 2, the error generally increases with the obstacle size, although it is not strictly monotonic.

The bearing angle error generally amplifies with increasing proximity of the obstacle to the sensors, but this trend is not universal. The effect of the normal-to-the-line (y) position of the obstacle is non-monotonic. In the case of the symmetric array, the largest error occurs when $y = \lambda$; this may be related to the differential diffraction of acoustic waves on the upper and lower edges and corners of the obstacle.

Figure 5 elucidates the effect of reducing the source-to-sensor distance keeping all other parameters unchanged. Here, the three sensors in the array are located at $(30, -1/2)$, $(30, 1/2)$ and $(30^2/3, 0)$, all coordinates being normalized by the pulse wavelength λ. With reference to table 1 and fig. 4, this constitutes a symmetric array of size λ, located 30λ away from the source.

The major difference is observed in the increased bearing angle estimation error incurred for the largest obstacle placed closest to the sensor array, and just off of the source-to-sensor line ($y = \lambda$). The error of 7.5° should be compared to the 3° error in the corresponding case with the farther sensor array in fig. 4. This could have been anticipated from fig. 2 – the distortion in the wavefront diminishes with distance behind the

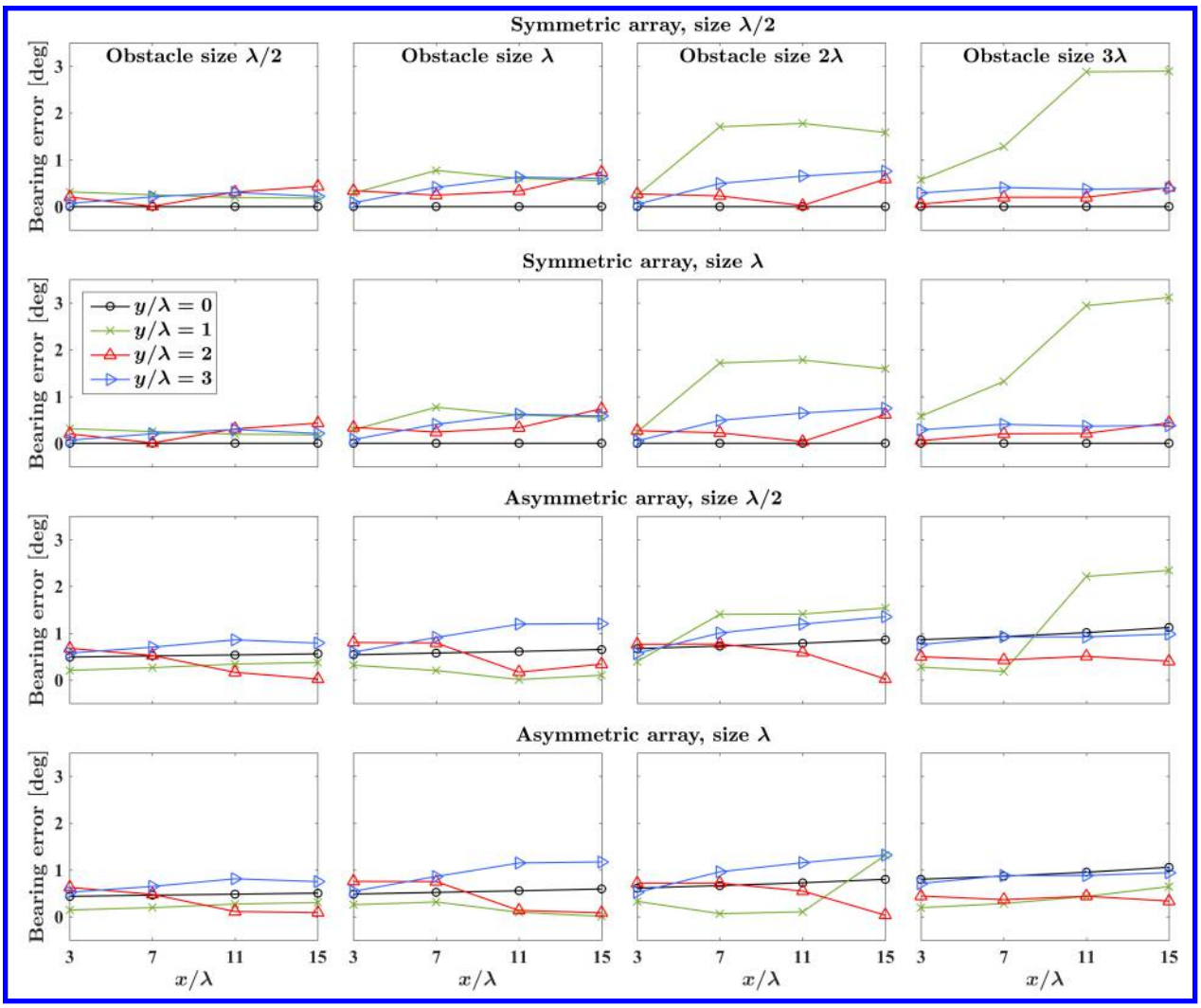

Figure 4: Bearing angle estimation error (in degrees) for a point source located at $(0, 0)$ and sensor arrays centred at $(48\lambda, 0)$, λ being the pulse wavelength. Each row corresponds to one of the four arrays described in table 1. Square obstacles of four sizes are tested as indicated at the top of each column. In each subplot, the error is plotted vs. the obstacle centroid position (x) along the line joining the source to the sensor array. The four curves in each subplot are for different normal-to-the-line distances of the obstacle center (y).

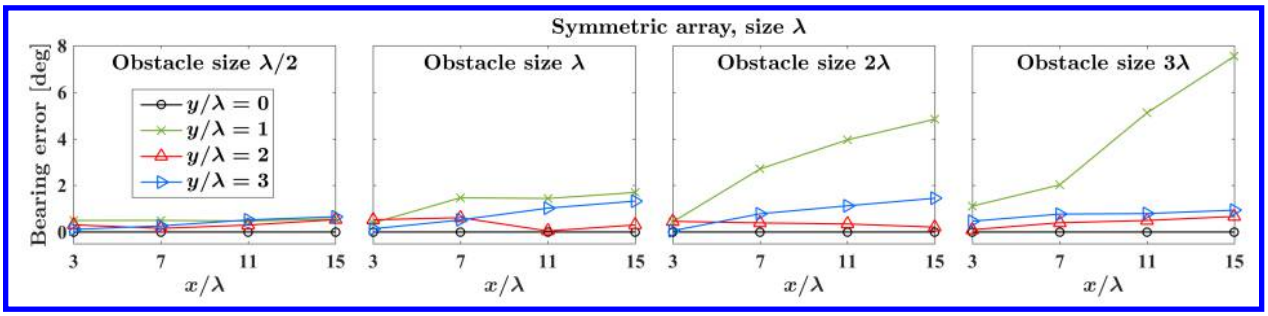

Figure 5: Bearing angle estimation error using a 'symmetric' sensor array of size λ centred at $(30\lambda, 0)$; refer to fig. 4 for further details.

obstacle. However, given the application of the localization technology, the overall errors in angle estimate

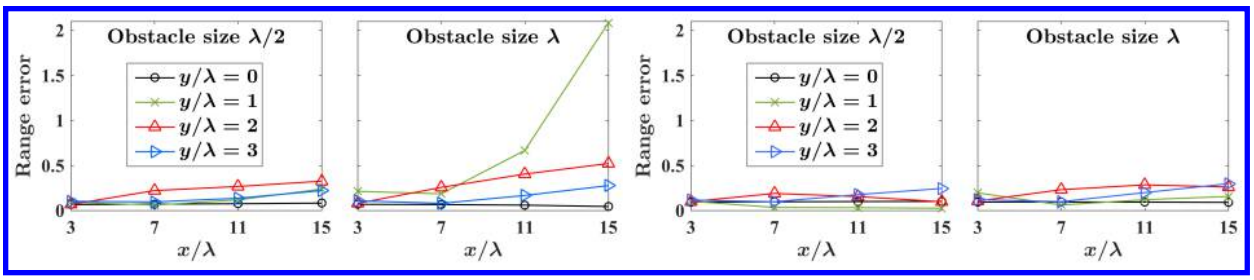

Figure 6: Range estimation errors normalized by the true range using a 'symmetric' sensor array of size λ centred at (a) $(30\lambda, 0)$, and (b) $(48\lambda, 0)$; refer to fig. 4 for further details.

may still be acceptable.

2. Range estimation error

The direction of propagation of the acoustic wavefront encountered by the sensor array determines the bearing angle estimate. On the other hand, the curvature of the wavefront is used to estimate the range of the source. The presence of an obstacle is known to distort the wavefront directly behind it. This explains the large errors in the range estimation presented in fig. 6. Even for the small obstacle of size $\lambda/2$, the maximum error reaches up to 30% of the true range. For the larger obstacle, the estimate worsens significantly in some cases. The errors are lower when the sensor is placed farther from the obstacle, due to the decrease of distortion of the wavefront with distance from the obstacle.

We omit presentation of range estimation results for larger obstacles (sizes 2λ and 3λ), since the trend towards worsening results are already demonstrated.

V. Conclusion

Real-time gunshot localization algorithms that use simultaneous recordings of the impulsive signature on multiple microphones typically assume that the muzzle blast wavefront is a sphere centred on the shooter. In this paper, we ascertain the validity of this assumption in the presence of intervening obstacles using numerical experiments. Our results indicate that the estimate of the bearing angle of the shooter is quite robust to obstacles, whereas the range estimate may be rendered very inaccurate. The bearing angle happens to be the information of greater importance in the relevant combat scenarios.

Acknowledgements: The authors acknowledge support from the National Center of Excellence in Technology for Internal Security (NCETIS) at Indian Institute of Technology Bombay.

References

[1] E. A. Page and B. Sharkey. SECURES: system for reporting gunshots in urban environments. *Proc. SPIE*, 2497:160–172, 1995.

[2] N. Sirola. Closed-form algorithms in mobile positioning: Myths and misconceptions. In *7th Workshop on Positioning navigation and communication (WPNC)*, pages 38–44, 2010.

[3] S. Bancroft. An algebraic solution of the GPS equations. *IEEE Transactions on Aerospace and Electronic Systems*, AES-21 (7):56–59, 1985.

[4] G. C. Carter. Time delay estimation for passive sonar signal processing. *IEEE Transactions on Acoustics, Speech, and Signal Processing*, 29(3):463–470, 1981.

[5] K. W. Lo and B. G. Ferguson. Localization of small arms fire using acoustic measurements of muzzle blast and/or ballistic shock wave arrivals. *J. Acoust. Soc. Am.*, 132(5):2997–3017, 2012.

[6] N. B. McNelis. Method and apparatus for determining the general direction of the origin of a projectile, US Patent 5,544,129, 1996.

[7] C. K. W. Tam and J. C. Webb. Dispersion-relation-preserving finite difference schemes for computational acoustics. *Journal of computational physics*, 107(2):262–281, 1993.

[8] C. K. W. Tam. *Computational aeroacoustics: a wave number approach*. Cambridge Univ Press, 2012.

[9] R. Maher. Modeling and signal processing of acoustic gunshot recordings. In *12th IEEE DSP Workshop & 4th IEEE Signal Processing Education Workshop*, pages 257–261, 2006.